LA-UR-17-24634 (Accepted Manuscript)

Low stress drop earthquakes in the rupture zone of the 1992 Nicaragua tsunami earthquake

Bilek, Susan L.
Rotman, Holly M. M.
Phillips, William Scott

To be published in: Geophysical Research Letters

DOI to publisher's version: 10.1002/2016GL070409

Permalink to record: http://permalink.lanl.gov/object/view?what=info:lanl-repo/lareport/LA-UR-17-24634

Low Stress Drop Earthquakes in the Region of the 1992 Nicaragua Tsunami Earthquake

Susan L. Bilek and Holly M. M. Rotman

Earth and Environmental Science Dept., New Mexico Tech, Socorro, NM, USA.

W. Scott Phillips

Los Alamos National Laboratory, Los Alamos, NM, USA.

Corresponding Author: S.L. Bilek, Earth and Environmental Science Dept., New Mexico Tech, Socorro, NM 87801, USA. (sbilek@nmt.edu)

Key Points:

1) Earthquake source parameters presented for 216 earthquakes along Pacific coast of Nicaragua and Costa Rica

2) Stress drop is lower for earthquakes within the 1992 tsunami earthquake rupture zone

3) Results suggest microseismicity can provide indication of anomalous rupture zones

Index Terms:

7215, 7230, 8170

Abstract

Tsunami earthquakes, events that generate larger than expected tsunami and are deficient in high frequency seismic radiation, are rare but hazardous to coastal populations. One model for these events is shallow rupture through low strength materials. We calculate source parameters of small magnitude earthquakes in the 1992 Nicaragua tsunami earthquake region to explore if fault conditions affect both small and large earthquakes. We determine seismic moment, corner frequency, and stress drop for 216 events between $2.1 < M_w < 4.7$ recorded in southern Nicaragua and northern Costa Rica from November 2005 to June 2006 using spectral ratios of narrow band envelopes (including coda). Mean stress drop of events within the rupture area is 1.2 MPa, and 5.5 MPa for events just outside of the rupture zone, with similar magnitude earthquakes in each group. Our results demonstrate different source parameter characteristics for microseismicity in the region of a past tsunami earthquake.

1. Introduction

Tsunami earthquakes are unusual earthquakes that generate significantly larger tsunami than would be expected for their moderate magnitude, have long rupture durations and low stress drop, thus tend to be deficient in high frequency seismic radiation [e.g. *Kanamori*, 1972; *Pelayo and Wiens,* 1992; *Kanamori and Kikuchi*, 1993; *Tanioka and Satake*, 1996; *Bilek and Lay,* 1999; 2002; *Polet and Kanamori*, 2000; *Ammon et al.,* 2006; *Yue et al.,* 2014]. These events are particularly hazardous in coastal regions because nearby communities are not alerted by the high frequency shaking that typically accompanies a large earthquake, and thus may fail to recognize the tsunami potential. Fatalities associated with these events can be significant, such as ~170 in the 1992 M_w=7.6 Nicaragua tsunami earthquake [e.g. *Velasco et al*., 1994], over 250 and 500 in

42 the 1994 M_s=7.2 Java [*Abercrombie et al.*, 2001] and 2010 M_w=7.8 Mentawai, Java events [*Hill*
43 *et al.*, 2012], respectively.

44 Given the tsunami hazard, there is a need to better characterize where these tsunami
45 earthquakes may occur. To date, only a handful of subduction zone segments have experienced
46 them. A commonly used model to explain these events involves shallow, near-trench slip
47 through low strength materials, likely made possible by highly heterogeneous fault friction
48 conditions [e.g. *Kanamori and Kikuchi*, 1993; *Geist and Bilek,* 2001; *Bilek and Lay*, 2002; *Lay et*
49 *al.*, 2012]. An important question is whether these conditions exist only in the small number of
50 regions that have documented cases, or if other subduction zones might also host them. The
51 difficulty in answering this question is the relatively small number of large magnitude events that
52 might sample the near-trench region of a given subduction zone. The use of more frequent
53 smaller magnitude earthquakes may be an appropriate substitute to sample the properties of a
54 given fault zone.

55 We test this idea by examining a dataset of well-recorded earthquakes that sample both
56 inside and adjacent to the 1992 Nicaragua tsunami earthquake rupture zone (Fig. 1). The 1992
57 Nicaragua tsunami earthquake was one of the first of this class of events to be recorded on
58 modern seismic instrumentation, clearly showing the lack of high frequency radiation, and
59 allowed for the extraction of source parameters such as slow rupture duration of ~110 s, low
60 stress drop, and relatively smooth slip distribution [e.g. *Kanamori and Kikuchi*, 1993; *Velasco et*
61 *al.*, 1994; *Ihmlé*, 1996]. If the fault conditions persist over time within the limited rupture zone,
62 then small earthquakes that sample the same area may also exhibit similar source properties.

63 **2. Data**

64 We use seismic data, sampled at 100 Hz, recorded by the short period land and ocean bottom
65 seismometer (OBS) network deployed from November 2005 to June 2006 as part of the German
66 SFB-574 project [*Dinc et al.* 2011] (Fig. 1). An original set of 279 earthquakes were selected for
67 study with a magnitude range of M_w 1.7 – 4.7, a depth range of 8-32 km, and hypocentral
68 location within 10 km of the USGS slab model [*Hayes et al.*, 2012]. The events were separated
69 into 3 geographic clusters using the MATLAB kmeans clustering function, a non-hierarchical
70 iterative algorithm used to separate our events into user-defined number of clusters by
71 minimizing the distance between points within each cluster. We analyze events by cluster to
72 reduce event-station path differences for added stability of the direct and coda wave (envelope)
73 spectral ratios. Our clusters separate into 3 distinct groups: c1 and c2 are located within the
74 southern extent of the 1992 tsunami earthquake rupture zone in a high moment release patch
75 defined by *Ihmlé* [1996]. The third cluster, c3, contains events located adjacent and outside the
76 1992 rupture zone. The rupture extent shown here from *Ihmlé* [1996] is similar to others
77 produced with different datasets [e.g. *Velasco et al.,* 1994; *Satake,* 1994].
78 After all data quality control and insufficient constraint removals were complete, our
79 final event distribution includes a total of 216 events. Cluster c1 contains 61 events with 2.1 <
80 M < 4.1, depth range 11.5-30 km and event separation between 0.1-109 km (median 17 km).
81 Cluster c2 contains 67 events, with 2.4 < M < 4.7, depth range 10-21 km, and event separation of
82 0.1-48 km (median 10.3 km). Cluster c3 contains 88 events with 2.2 < M < 4.4, depth range of 3-
83 16 km, and event separation 0.1-69 km (median 10.7 km).
84 As the first quality control step, we examined seismograms for high signal to noise ratio
85 and identifiable direct arrivals with no additional events observable in the time window. For
86 events passing this step, we computed narrow band velocity envelopes from both horizontal

87 components (Fig. 2a). The seismograms are de-meaned, tapered, bandpassed with 2-pole
88 Butterworth filters, then Hilbert transformed to obtain envelopes for 15 sub-octave frequency
89 bands between 0.2 and 48 Hz. Individual band widths range from 0.1 to 16 Hz. Because land and
90 OBS data were recorded at the same sample rates, all seismograms were treated the same.

91 **3. Spectral Ratio Method**

92 Preliminary steps for spectral ratio calculation include pre-processing envelopes based on
93 signal to noise ratio (SNR) relative to the background noise level before the P arrival. We require
94 envelope SNR of a minimum of 2; envelopes for event pairs that met this criteria were used to
95 determine source ratios for each band. Events in a pair consist of any events in the cluster with
96 at least one common station and narrowband frequency envelope. Median event separations for
97 each cluster (horizontal and depth separation of 17 km and 10 km (c1), 10 km and 8 km (c2) and
98 11 km and 6 km (c3) respectively) are within commonly used ranges for previous spectral ratio
99 studies [e.g. Malagnini and Mayeda, 2008; Mayeda and Malagnini, 2009; Baltay et al, 2010]

100 Stress drop ($\Delta\sigma$) using *Madariaga* [1976], corner frequency (f_c), and seismic moment
101 (M_o) are determined from the source spectral ratios of the envelopes, which are dominated by the
102 S-coda. Coda waves are scattered off heterogeneities along indirect paths between the source
103 and receiver [e.g., *Aki*, 1969; *Aki and Chouet*, 1975], and the coda amplitudes are stable with
104 respect to epicentral distance, azimuth, source mechanism, and laterally varying path effects
105 [e.g., *Aki*, 1969; *Aki and Chouet*, 1975; *Rautian and Khalturin*, 1978; *Phillips and Aki*, 1986;
106 *Mayeda et al.*, 2007; *Mayeda and Malagnini*, 2010]. Source parameter results based on data from
107 coda are similar to those based on direct wave data, with reduced scatter in the spectral ratios
108 [e.g. *Mayeda et al.*, 2007; *Mayeda and Malagnini*, 2010; *Abercrombie*, 2013; *Fisk and Phillips*,
109 2013; *Yoo and Mayeda*, 2013; *Somei et al.*, 2014]. We use the spectral ratio method described

by *Mayeda et al.* [2007], which has been further developed in more recent studies [e.g., *Phillips et al*., 2008; *Moyer et al*., 2011; *Fisk and Phillips*, 2013].

For each event pair, and each station and band, we collect median envelope differences in time windows following the P-wave arrival and where the SNR is at least 2. We combine all stations within the event pairs to compute the source spectral ratios. We use the *Brune* [1970] ω-squared model to solve for the source parameters (moment and corner frequency) for all events in one cluster, using an independently determined moment to set the absolute level. For one spectral ratio, the ω-squared model predicts

$$\frac{S_1(f)}{S_2(f)} = \frac{M_o^{(1)}[1 + (\frac{f}{f_c^{(2)}})^2]}{M_o^{(2)}[1 + (\frac{f}{f_c^{(1)}})^2]} \quad (1)$$

where S represents event spectra, f is the frequency, M_o is event seismic moment, f_c is event corner frequency, and indices 1 and 2 represent the larger and smaller event in the pair, respectively [e.g. *Fisk and Phillips*, 2013].

Using at least one well constrained seismic moment per cluster is critical for final source parameter solutions [e.g. *Mayeda et al*., 2007, *Yoo et al.,* 2013]. For each of the 3 events we use as independent constraints, we have 3 reported magnitude estimates from various national and international catalogs (Table S1). In addition, we perform independent calibration for each of these events by computing P-wave spectra using the approach of *Brune* [1970] and *Abercrombie* [1995] and utilizing broadband land stations with signal to noise ratio of at least five and hypocentral distance of 60-155 km. We use a 10 s window containing the P wave on vertical component of the displacement seismogram, convert to a displacement spectrum, and compare with theoretical P-wave spectra determined with the equation:

$$\Omega(f) = \frac{\Omega_0 e^{\frac{-\pi f t}{Q}}}{[1 + (\frac{f}{f_c})^{\gamma n}]^{\frac{1}{\gamma}}} \quad (2)$$

where Ω is the amplitude, t is the travel time, Q is the quality factor (500, *Dorman et al.* [2003]), γ is a constant set to 1, and n is the falloff rate at high frequencies (set to 2) [*Abercrombie*, 1995]. Seismic moment was then determined with the equation:

$$M_o = \frac{4\pi\rho c^3 D\sqrt{\Omega(Z)^2}}{R_{\theta\varphi p}} \quad (3)$$

where M_o is seismic moment, ρ is density (2700 kg/m^3), c is P-wave velocity (6000 m/s), D is the hypocentral distance in meters, Ω is the amplitude for the vertical component, and $R_{\theta\varphi P}$ is the P-wave radiation pattern (0.44) [*Brune*, 1970; *Abercrombie*, 1995]. Our resulting magnitudes are very similar to the catalog reported values (Table S1).

We used a non-linear, iterative, least squares inversion routine to obtain source parameters from the assembled spectral ratio data. The model and starting values assumed omega-squared behavior at higher frequencies and a flat spectrum below the corner frequency (Equation 1). Data residuals more than three standard deviations from an initial fitted model were trimmed between two inversion steps. The final source parameters are the best fit (Fig. 2b) by iterative least squares among all the event pairs, and the resulting spectral ratio plots for each pair are visually examined after inversion to verify the automatic fitting process and confirm that both event f_c are constrained by at least 2 spectral ratio amplitudes at higher and lower frequencies.. The results presented here have ~3.5 orders of magnitude variation in seismic moment in each cluster.

We also estimate uncertainties in f_c and M_o resulting from the distribution of events and event pairs for each cluster using a jack-knife technique, removing 1 event from the cluster and

152 re-inverting the remaining events. We perform this removal and new iteration for each event
153 within the cluster, with the sole exception of the event with the independently constrained
154 moment. We use the population of f_c and M_o results from the suite of inversions for each cluster
155 to find the average and standard deviation of these values, with the standard deviation reported in
156 the error bars for these parameters (Fig. 3).
157 For events that pass the above constraints, we compute stress drop ($\Delta\sigma$) based on
158 *Madariaga* [1976]:

159 $$\Delta\sigma = M_o(\frac{f_c}{0.42\beta})^3 \quad (4)$$

160 where β is the S-wave velocity, set to 3500 m/s. This is within the range of 3000 – 4000 m/s
161 used with previous calculations of Madariaga stress drop [*Izutani*, 2005; *Shearer et al.*, 2006;
162 *Allmann and Shearer*, 2009], and is reasonable based on velocity models near the Middle
163 America trench in Nicaragua and Costa Rica [*DeShon et al.*, 2006; *Harmon et al*., 2013].
164 **4. Source Parameter Results**
165 For our final dataset of 216 well-constrained events, we find that corner frequency varies
166 from ~1.2 Hz to 18 Hz (constrained by data) and seismic moment ranges from $2x10^{12}$ N-m to
167 $1.6x10^{16}$ N-m (M_w 2.1-4.7) (Fig. 3). Earthquake stress drops (Equation 4) fall generally within
168 expected ranges of earthquake stress drop found globally, largely between 0.1-10 MPa, with a
169 mean of 2.9 MPa, comparable to global mean stress drop of 3 MPa, but larger than the mean of
170 0.8 MPa determined for larger magnitude subduction zone events in Costa Rica and southern
171 Nicaragua [*Allmann and Shearer*, 2009].
172 There is a clear difference in results for events within the 1992 rupture and those events
173 outside of the rupture zone, with those events in clusters c1 and c2 inside the rupture zone having
174 lower corner frequency and stress drop than for those events in cluster c3 outside of the rupture

zone. The clusters of events within the southern extent of the 1992 rupture (n=128) (Fig. 4) have overall mean stress drop of 1.2 MPa (with 1 standard deviation of 2.6 MPa) and mean corner frequency of 4.9 Hz. Separately examining the rupture area clusters, we find the downdip cluster, c1, (n = 61) has mean corner frequency of 5.5 Hz and mean stress drop of 0.8 MPa, and the cluster nearest to the high slip zone, c2 (n = 67) has mean corner frequency and stress drop of 4.4 Hz and 1.5 MPa respectively. The cluster (n = 88) south of the 1992 rupture has a mean corner frequency and stress drop of 9.2 Hz and 5.5 MPa respectively.

We lack focal mechanism information for these events, but assume that they are interplate thrust mechanism based on the applied event selection criteria of proximity to the seismically defined slab interface. If this assumption is not correct for all events, we may see the effect of different fault type in the stress drop measurements, as indicated by *Allmann and Shearer* [2009] who find higher stress drops, by a factor of ~2, for intraplate events relative to interplate events. Stress drop outside the rupture zone is ~4.5x larger than inside the rupture zone. Using clusters c2 and c3 as they have similar distance from the trench, we find that c3 has 3.6x larger stress drop than c2 inside the rupture zone, thus even the different focal mechanisms could not explain this difference [e.g. *Choy and Boatwright*, 1995]. Additionally, it would be unlikely that all the higher stress drop events outside the rupture area would be dominantly intraplate, as thrust mechanism earthquakes of a range of magnitudes have been documented in northern Costa Rica [e.g. *Hansen et al.,* 2006; *Yue et al.,* 2013; *Protti et al.*, 2014].

A few possible reasons for the variations in f_c and thus stress drop could include bandwidth issues [e.g. *Ide and Beroza*, 2001; *Abercrombie,* 2013], inadequate removal of path effects, or station bias. All seismic stations used in the study were recorded at 100 Hz, thus we do have adequate bandwidth to sample f_c for the smaller events in our study. Path effects should

198 be removed adequately given our event separation distances. The distribution of OBS vs land
199 stations used may also cause bias, however OBS records make up 43% of the envelopes used for
200 cluster c1, 77% of cluster c2, and 67% of cluster c3. One might expect that noisy OBS records
201 might lead to higher frequency characteristics in the envelopes and higher fc estimates, but we
202 use the most OBS records in one of the clusters inside the rupture area, not outside. Thus we do
203 not believe that these issues cause significant bias in our results.

204 **5. Discussion**

205 Our results show a distinct difference in the high frequency radiation of events that
206 occurred within the rupture area of the 1992 Nicaragua tsunami earthquake to those events that
207 occurred just outside of the rupture zone. Earthquake corner frequencies can be related to
208 rupture velocity or stress drop. We have used the corner frequencies to compute stress drop and
209 highlight spatial variations, but we could also turn these corner frequencies into rupture durations
210 and rupture velocities. Our results then would suggest low rupture velocities for those events
211 within the 1992 rupture zone.

212 The 1992 tsunami earthquake had a very low rupture velocity, ~0.6-1 km/s [*Velasco et*
213 *al.,* 1994*; Imhle,* 1996]. Stress drop estimates for the 1992 event range from 0.01-0.07 MPa
214 [*Velasco et al.,* 1994], 1.1 MPa [*Kikuchi and Kanamori*, 1995] to between 3-7 MPa [*Imhlé,*
215 1996]. *Convers and Newman* [2011] use large magnitude earthquakes to show that the entire
216 Nicaragua/Costa Rica margin hosts earthquakes that lack high frequency radiation relative to
217 global averages. However, their large earthquake catalog does not have the spatial sampling to
218 resolve the fine-scale details about behavior within and adjacent to the 1992 rupture patch. Other
219 tsunami earthquakes have also been described as having low rupture velocities and/or stress
220 drops, such as events in Peru, Sumatra, Java, Kuriles, Japan, and Solomon Islands [e.g. *Polet and*

221 *Kanamori*, 2000; *Yue et al.,* 2014; *Ammon et al.,* 2006*; Pelayo and Wiens,* 1992; *Tanioka and*
222 *Satake*, 1996; *Newman et al.,* 2011].

223 Various studies have linked stress drops and rupture velocity variations to specific
224 conditions on the fault. Recent work suggests pore pressure increases near fluid injection sites
225 lead to lower stress drops for small magnitude induced earthquakes [e.g. *Goertz-Allmann et al.*,
226 2011]. *Oth* [2013] finds spatial variations of stress drop along Japan linked to thermal variations
227 and geodetic coupling. Along Nicaragua and northern Costa Rica, heat flow data are limited, but
228 do not show significant spatial differences over the scale of our study area [*Harris et al.,* 2010].
229 Other studies link variations in stress drop to variations in fault weakening, tied to high-speed
230 laboratory friction experiments [e.g. *Malagnini et al.,* 2014] or past seismic activity [e.g.
231 *Allmann and Shearer,* 2007]. Tsunami earthquake models have stressed the importance of the
232 shallow slip in low strength sedimentary fault materials as a way to reduce rupture velocities for
233 the near-trench slip. The Nicaragua portion of the Middle America trench region has been
234 classified as an erosive plate margin [e.g. *Clift and Vannucchi,* 2004], with the Cocos Plate
235 significantly faulted as it enters the trench [*Ranero et al*, 2003] and the presence of subducted
236 seamounts at depth [*McIntosh et al.*, 2007]. The plate bending faults have been suggested as an
237 effective conduit for fluid flow up into the plate boundary fault and upper plate [e.g. *Ranero et*
238 *al.*, 2003; *Salleres et al.*, 2013, *Thorwart et al.,* 2014], and allows for sediment-filled half
239 grabens to enter the seismogenic zone. The seamount at 8-10 km depth in the area of high slip
240 during the 1992 tsunami earthquake leads to significant upper plate fracturing [*McIntosh et al.,*
241 2007]; all of the features described above would introduce heterogeneity into the fault and
242 earthquake rupture process. *Carpenter et al.* [2014] highlight particular heterogeneities, such as
243 lithology and fault contacts, within fault rocks representative of seismogenic depths that lead to

244 frictional and slip heterogeneities during rock friction experiments, linking to variations in
245 rupture times in earthquakes. We suggest that heterogeneity along the Nicaragua margin,
246 including the upper plate fracturing, sediment-filled grabens, and likely high fluid pressure down
247 to ~20 km depth and 65 km landward of the trench also leads to earthquakes of lower corner
248 frequencies/lower stress drops. The events in our study are small enough magnitude to have not
249 produced displacements large enough to generate tsunami, as the 1992 tsunami earthquake did.
250 The results of our study does not answer the question of what specific condition or
251 process leads to the low stress drop or rupture velocity observed along this segment of the
252 Central American subduction zone. However, it does point to the effectiveness of using the
253 more frequent small magnitude earthquakes as a probe for where these conditions or processes
254 may exist in the shallow subduction zone environment, an important constraint for assessing
255 hazard from tsunami earthquakes.

256 **6. Conclusions**

257 Our results suggest a significant spatial difference in earthquake corner frequency for 216
258 small magnitude earthquakes, indicating either low stress drop or low rupture velocities for
259 events that occurred within the rupture zone of the anomalous 1992 Nicaragua tsunami
260 earthquake. We find a sharp transition over a few 10s of km to larger corner frequencies (and
261 thus rupture velocity or stress drop) for events outside of the rupture zone. These events occur in
262 an area of a subducted seamount, significant upper plate deformation, and likely high fluid
263 pressures. Our results suggest these spatial variations in the fault rock conditions affect rupture
264 velocity and/or stress drop over a range of earthquake magnitudes.

265

266 **Acknowledgements**

The work was supported by NSF EAR-1141898. The NICAT network data was provided by the SFB574 project of the University of Kiel (Kiel, Germany) through Dr. Wolfgang Rabbel. The seismometers of the NICAT network were provided by the Geophysical Instrument Pool of the GFZ Potsdam (GIPP). We used the Seismic Analysis Code (SAC) and Generic Mapping Tools (GMT) for seismogram analysis and plotting. Waveforms were made available from H. DeShon and the relocated earthquake hypocenter catalogs were provided by M. Moore-Driskell.

References

Abercrombie, R. E. (1995), Earthquake source scaling relationships from −1 to 5 ML using seismograms recorded at 2.5-km depth, *J. Geophys. Res., 100*, 24015–24036.

Abercrombie, R.E. (2013), Comparison of direct and coda wave stress drop measurements for the Wells, Nevada, earthquake sequence, *J. Geophys. Res., 118*, 1458–1470, doi:10.1029/2012JB009638.

Abercrombie, R.E., M. A. Antolik, K. R. Felzer, and G. Ekström (2001), The 1994 Java earthquake: slip over a subducting seamount, *J. Geophys. Res., 106*, 6595-6607.

Aki, K. (1969), Analysis of the seismic coda of local earthquakes as scattered waves, *J. Geophys. Res., 74*, 615-631.

Aki, K., and B. Chouet (1975), Origin of coda waves: source, attenuation, and scattering effects, *J. Geophys. Res., 80*, 3322-3342.

Allmann, B. P., and P. M. Shearer (2007), Spatial and temporal stress drop variations in small earthquakes near Parkfield, California, *J. Geophys. Res., 112*, B04305, doi:10.1029/2006jb004395.

Allmann, B. P., and P. M. Shearer (2009), Global variations of stress drop for moderate to large earthquakes, *J. Geophys. Res., 114*, B01310, doi:10.1029/2008JB005821.

Ammon, C. J., H. Kanamori, T. Lay, and A. A. Velasco (2006), The 17 July 2006 tsunami earthquake, *Geophys. Res. Lett., 33*, L24308, doi:10.1029/2006GL028005.

Bilek, S. L., and T. Lay (1999), Rigidity variations with depth along interplate megathrust faults in subduction zones, *Nature, 400*, 443-446.

Bilek, S. L., and T. Lay (2002), Tsunami earthquakes possibly widespread manifestations of frictional conditional stability, *Geophys. Res. Lett., 29*, doi:10.1029/2002GL015215.

Brune, J.N. (1970), Tectonic stress and the spectra of seismic shear waves from earthquakes, *J. Geophys. Res., 75(26)*, 4997-5009.

Carpenter, B. M., M. M. Scuderi, C. Collettini, and C. Marone (2014), Frictional heterogeneities on carbonate-bearing normal faults: Insights from the Monte Maggio Fault, Italy, *J. Geophys. Res, 119*, doi:10.1002/2014JB011337.

Choy, G.L., and J.L. Boatwright (1995), Global patterns of radiated seismic energy and apparent stress, *Journal of Geophysical Research, 100*(B9), 18205-18228.

Clift, P., and P. Vannucchi (2004), Controls on tectonic accretion versus erosion in subduction zones: Implications for the origin and recycling of the continental crust, *Rev. Geophys., 42*, doi:10.1029/2003rg000127.

Convers, J. A., and A. V. Newman (2011), Global evaluation of large earthquake energy from 1997 through mid‐2010, *J. Geophys. Res., 116*, B08304, doi:10.1029/2010JB007928.

DeShon, H.R., S.Y. Schwartz, A.V. Newman, V. Gonzalez, M. Protti, L.M. Dorman, T.H. Dixon, D.E. Sampson, and E.R. Flueh (2006), Seismogenic zone structure beneath the Nicoya Peninsula, Costa Rica, from three-dimensional local earthquake P- and S-wave tomography, *Geophys. J. Int., 164*, 109-124, doi:10.1111/j.1365-246X.2005.02809.x.

Dinc, A. N., Rabbel, W., Flueh, E. R., & Taylor, W. (2011). Mantle wedge hydration in Nicaragua from local earthquake tomography. *Geophysical Journal International, 186*, 99-112.

Dorman, L., A. Sauter, S. Schwartz, H. DeShon, A. Newman, M. Protti, S. Bilek, E. Flueh, and T. Dixon (2003), Seismic attenuation in the subduction zone of Costa Rica, MARGINS Theoretical Institute on the Seismogenic Zone Experiment, Snowbird, UT.

Fisk, M.D., and W.S. Phillips (2013), Constraining regional phase amplitude models for Eurasia, Part 1: Accurate source parameters and geometric spreading, *Bull. Seismo. Soc. Am., 103*, 3248-3264, doi:10.1785/0120130018.

Geist, E.L., and S.L. Bilek (2001), Effect of depth-dependent shear modulus on tsunami generation along subduction zones, *Geophys. Res. Lett.*, *28*, 1315-1318.

Goertz-Allmann, B. P., A. Goertz, and S. Wiemer (2011), Stress drop variations of induced earthquakes at the Basel geothermal site, *Geophys. Res. Lett., 38*, L09308, doi:10.1029/2011gl047498.

Hansen, S. E., S. Y. Schwartz, H. R. DeShon, and V. Gonzalez (2006), Earthquake relocation and focal mechanism determination using waveform cross correlation, Nicoya Peninsula, Costa Rica, *Bull. Seismo. Soc. Am., 96*, 1003-1011, doi:10.1785/0120050129.

Harmon, N., M. S. De La Cruz, C. A. Rychert, G. Abers, and K. Fischer (2013), Crustal and mantle shear velocity structure of Costa Rica and Nicaragua from ambient noise and teleseismic Rayleigh wave tomography, *Geophys. J. Int., 195*, 1300-1313, doi:10.1093/gji.ggt309.

Harris, R. N., I. Grevemeyer, C. R. Ranero, H. Villinger, U. Barckhausen, T. Henke, C. Mueller, and S. Neben (2010), Thermal regime of the Costa Rican convergent margin: 1. Along-strike variations in heat flow from probe measurements and estimated from bottom-simulating reflectors, *Geochem. Geophys. Geosyst*., , doi:10.1029/2010GC003272.

Hayes, G. P., D. J. Wald, and R. L. Johnson (2012), Slab1.0: A three-dimensional model of global subduction zone geometries, *J. Geophys. Res., 117*, B01302, doi:10.1029/2011jb008524.

Hill, E. M., et al. (2012), The 2010 Mw 7.8 Mentawai earthquake: Very shallow source of a rare tsunami earthquake determined from tsunami field survey and near-field GPS data, *J. Geophys. Res., 117*, B06402, doi:10.1029/2012jb009159.

Ide, S., and G. C. Beroza (2001). Does apparent stress vary with earthquake size?, *Geophysical Research Letters 28* 3349-3352.

Ihmle, P. F. (1996), Monte Carlo slip inversion in the frequency domain: Application to the 1992 Nicaragua slow earthquake, *Geophys. Res. Lett., 23*, 913-916.

Izutani, Y. (2005), Radiated energy from the mid Niigata, Japan, earthquake of October 23, 2004, and its aftershocks, *Geophys. Res. Lett., 32*, doi:L21313 10.1029/2005gl024116.

Kanamori, H. (1972), Mechanism of tsunami earthquakes, *Phys. Earth Planet. Int., 6*, 246-259.

Kanamori, H., and M. Kikuchi (1993), The 1992 Nicaragua earthquake: A slow tsunami earthquake associated with subducted sediments, *Nature, 361*, 714-716.

Kikuchi, M., and H. Kanamori (1995), Source Characteristics of the 1992 Nicaragua Tsunami Earthquake Inferred from Teleseismic Body Waves, *Pure and Applied Geophys*., *144*, 441-453.

Lay, T., H. Kanamori, C. J. Ammon, K. D. Koper, A. R. Hutko, L. L. Ye, H. Yue, and T. M. Rushing (2012), Depth-varying rupture properties of subduction zone megathrust faults, *J. Geophys. Res., 117*, B04311,doi:10.1029/2011jb009133.

Madariaga, R. (1976), Dynamics of an expanding circular fault, *Bull. Seismo. Soc. Am., 66*, 639-666.

Malagnini, L., K. Mayeda, S. Nielsen, S.-H. Yoo, I. Munafo', C. Rawles, and E. Boschi (2014), Scaling Transition in Earthquake Sources: A Possible Link Between Seismic and Laboratory Measurements, *Pure and Applied Geophys*., *171*, 2685-2707, doi:10.1007/s00024-013-0749-8.

Mayeda, K., L. Malagnini, and W. R. Walter (2007), A new spectral ratio method using narrow band coda envelopes: Evidence for non-self-similarity in the Hector Mine sequence, *Geophys. Res. Lett., 34*, L11303, doi:10.1029/2007GL030041.

Mayeda, K., and L. Malagnini (2010), Source radiation invariant property of local and near-regional shear-wave coda: Application to source scaling for the Mw 5.9 Wells, Nevada sequence, *Geophys. Res. Lett., 37*, L07306, doi:10.1029/2009GL042148.

McIntosh, K.D., E.A. Silver, I. Ahmed, A. Berhorst, C.R. Ranero, R.K. Kelly, and E.R. Flueh (2007), The Nicaragua convergent margin: Seismic reflection imaging of the source of a tsunami earthquake, in The Seismogenic Zone Of Subduction Thrust Faults, edited by T. H. Dixon and J. C. Moore, pp. 257-287, Columbia University Press, New York.

Moyer, P. A., S. L. Bilek, and W. S. Phillips (2011), Apparent stress variations near the Osa Peninsula, Costa Rica, influenced by subducted bathymetric features, *Geophys. Res. Lett., 38*, L02304, doi:10.1029/2010GL045955.

Newman, A. V., L. Feng, H. M. Fritz, Z. M. Lifton, N. Kalligeris, and Y. Wei (2011), The energetic 2010 MW 7.1 Solomon Islands tsunami earthquake, *Geophys. J. Int., 186*, 775-781.

Oth, A. (2013), On the characteristics of earthquake stress release variations in Japan, *Earth Planet. Sci. Lett., 377–378*, 132-141, doi:10.1016/j.epsl.2013.06.037.

Pelayo, A. M., and D. A. Wiens (1992), Tsunami earthquakes - Slow thrust-faulting events in the accretionary wedge, *J. Geophys. Res*., *97*, 15321-15337.

Phillips, W.S., and K. Aki (1986), Site amplification of coda waves from local earthquakes in central California, *Bull. Seism. Soc. Am*., **76**, 627-648.

Phillips, W.S., R. J. Stead, G.E. Randall, H.E. Hartse, and K.M. Mayeda (2008), Source effects from broad area network calibration of regional distance coda waves, in Earth heterogeneity and scattering effects on seismic waves, Advances in Geophysics, vol. 50, edited by H. Sato, M. Fehler, and R. Dmowska, pp. 319-351, Elsevier Inc., Burlington, MA.

Polet, J., and H. Kanamori (2000), Shallow subduction zone earthquakes and their tsunamigenic potential, *Geophys. J. Int., 142*, 684-702.

Protti, M., V. Gonzalez, A. V. Newman, T. H. Dixon, S. Y. Schwartz, J. S. Marshall, L. Feng, J. I. Walter, R. Malservisi, and S. E. Owen (2014), Nicoya earthquake rupture anticipated by geodetic measurement of the locked plate interface, *Nature Geosci, 7*, 117-121, doi:10.1038/ngeo2038.

Ranero, C. R., J. P. Morgan, K. McIntosh, and C. Reichert (2003), Bending-related faulting and mantle serpentinization at the Middle America trench, *Nature, 425*, 367-373.

Rautian, T.G., and V. I. Khalturin (1978), The use of the coda for determination of the earthquake source spectrum, *Bull. Seismo. Soc. Am., 68*, 923-948.

Sallarès, V., A. Meléndez, M. Prada, C. R. Ranero, K. McIntosh, and I. Grevemeyer (2013), Overriding plate structure of the Nicaragua convergent margin: Relationship to the seismogenic zone of the 1992 tsunami earthquake, *Geochem., Geophys., Geosys, 14*, 3436-3461, doi:10.1002/ggge.20214.

Satake, K. (1994). Mechanism of the 1992 Nicaragua Tsunami Earthquake, *Geophysical Research Letters 21* 2519-2522.

Shearer, P. M., G. A. Prieto, and E. Hauksson (2006), Comprehensive analysis of earthquake source spectra in southern California*, J. Geophys. Res., 111*, B06303, doi:10.1029/2005jb003979.

Somei, K., K. Asano, T. Iwata, and K. Miyakoshi (2014), Source Scaling of Inland Crustal Earthquake Sequences in Japan Using the S-Wave Coda Spectral Ratio Method, *Pure Appl. Geophys., 171*, 2747-2766, doi:10.1007/s00024-014-0774-2.

Thorwart, M., Y. Dzierma, W. Rabbel, and C. Hensen (2014), Seismic swarms, fluid flow and hydraulic conductivity in the forearc offshore North Costa Rica and Nicaragua, *Int. J. Earth Sci. 103*, 1789-1799, doi:10.1007/s00531-013-0960-y.

Tanioka, Y., and K. Satake (1996), Fault parameters of the 1896 Sanriku tsunami earthquake estimated from tsunami numerical modeling, *Geophys. Res. Lett., 23*, 1549-1552.

Velasco, A. A., C. J. Ammon, T. Lay, and J. Zhang (1994), Imaging a slow bilateral rupture with broadband seismic waves: The September 2, 1992 Nicaraguan tsunami earthquake, *Geophys. Res. Lett., 21*, 2629-2632.

Walter, W. R., and S. R. Taylor (2001), A revised magnitude and distance amplitude correction (MDAC2) procedure for regional seismic discriminants: Theory and testing at NTS, Rep. UCRL-ID-146,882, Lawrence Livermore Natl. Lab., Livermore, CA, http://www.llnl.gov/tid/lof/documents/pdf/240563.pdf.

Yoo, S-H., and K. Mayeda (2013), Validation of non-self-similar source scaling using ground motions from the 2008 Wells, Nevada, earthquake sequence, *Bull. Seismo. Soc. Am., 103*, 2508-2519, doi:10.1785/0120120327.

Yue, H., T. Lay, L. Rivera, Y. Bai, Y. Yamazaki, K. F. Cheung, E. M. Hill, K. Sieh, W. Kongko, and A. Muhari (2014), Rupture process of the 2010 Mw 7.8 Mentawai tsunami earthquake from joint inversion of near-field hr-GPS and teleseismic body wave recordings constrained by tsunami observations, *J. Geophys. Res., 119*, 2014JB011082, doi:10.1002/2014JB011082.

Yue, H., T. Lay, S. Y. Schwartz, L. Rivera, M. Protti, T. H. Dixon, S. Owen, and A. V. Newman (2013), The 5 September 2012 Nicoya, Costa Rica Mw 7.6 earthquake rupture process from joint

inversion of high-rate GPS, strong-motion, and teleseismic P wave data and its relationship to adjacent plate boundary interface properties, *J. Geophys. Res., 118*, 1-14, doi:10.1002/jgrb.50379.

Figure Captions:

Figure 1: Map of earthquakes and seismic network (solid triangle) along Nicaragua and northern Costa Rica, recording during November 2005 – June 2006. Earthquake analysis clusters are denoted c1 (red solid circles), c2 (red open circles), and c3 (black squares). Epicenter (star, USGS NEIC), Centroid Moment Tensor (www.globalcmt.org), rupture area (dashed box) and largest moment release (shaded ovals) from *Ihmlé* [1996]) are shown for the 1992 M_w=7.2 tsunami earthquake. Middle America Trench (MAT) and convergence rate shown for Cocos Plate.

Figure 2: Data processing for January 23, 2006 M_w 2.5 earthquake (cluster c1). a) Envelopes for selected frequency bands 0.5-48 Hz Hz for same event and land station NY11. P and S arrivals are marked with vertical bar. b) Resulting source ratios (open circles) for 2 events, one based on the envelopes shown in a. Solid lines (red) indicate best fit modeled source ratios based on the Brune model, solid circles (red) indicate best fit corner frequency for each event.

Figure 3: Log moment as function of corner frequency for all events analyzed. Solid lines indicate values of constant stress drop. Events located outside the 1992 rupture area (solid squares) have higher f_c and higher $\Delta\sigma$ than events located inside the 1992 rupture area (open circles). Error bars indicate one standard deviation about the mean f_c and M_o resulting from jackknife-based analysis.

513 Figure 4: Earthquake stress drop along northern Costa Rica and southern Nicaragua, spanning
514 the southern portion of the 1992 tsunami earthquake rupture zone. Earthquakes outside of the
515 rupture zone (dashed box) have higher $\Delta\sigma$ than those inside the rupture zone. The area of c1 and
516 c2 is within a low rupture velocity, high moment release patch of *Ihmlé* [1996]; this is also the
517 area of imaged subducted seamount [*McIntosh et al.*, 2007].

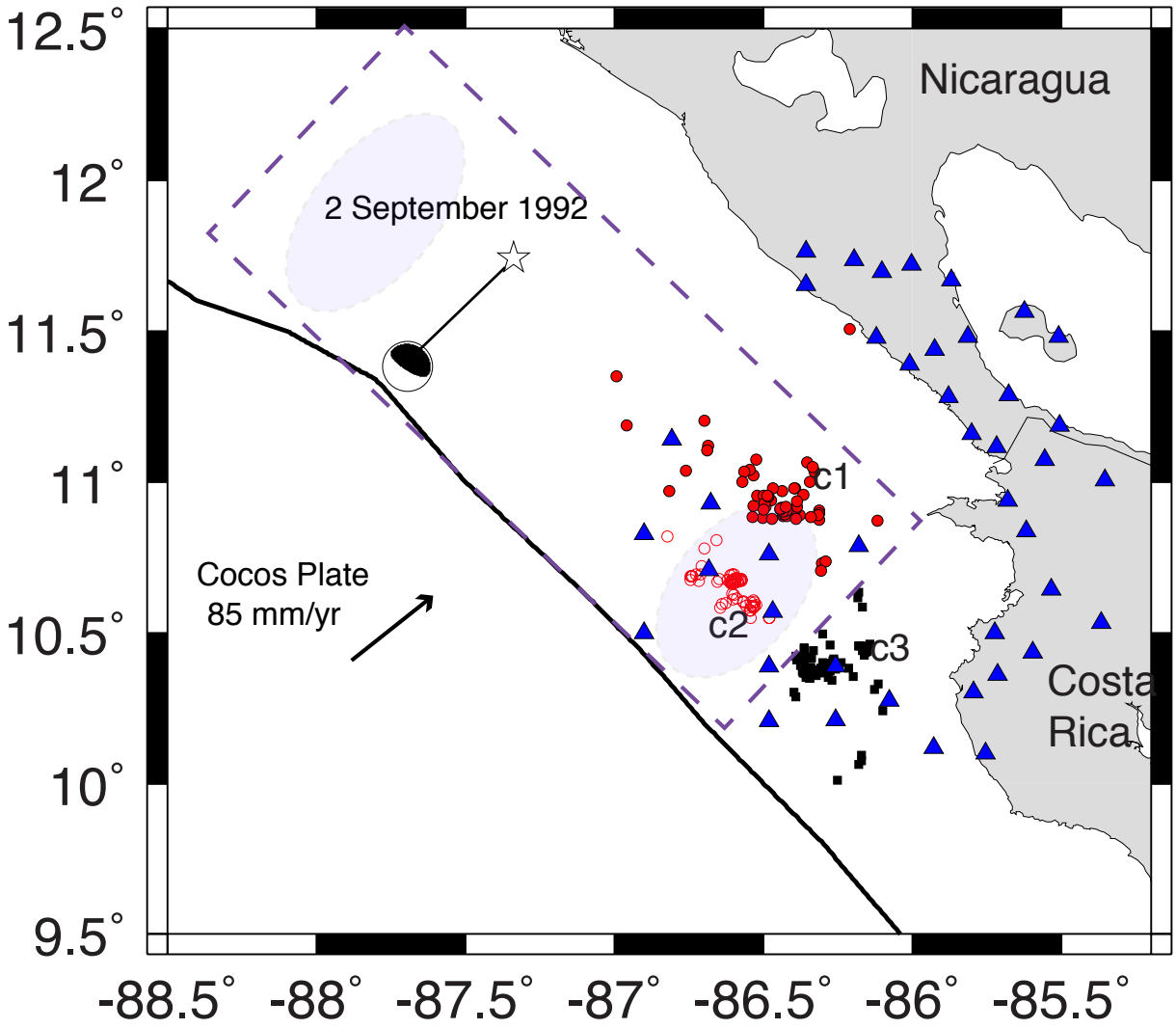

Figure 1. Map of earthquakes and seismic network (solid triangle) along Nicaragua and northern Costa Rica, recording during November 2005 – June 2006. Earthquake analysis clusters are denoted c1 (red solid circles), c2 (red open circles), and c3 (black squares). Epicenter (star, USGS NEIC), Centroid Moment Tensor (www.globalcmt.org), rupture area (dashed box) and largest moment release (shaded ovals) from Ihmlé [1996]) are shown for the 1992 Mw=7.2 tsunami earthquake. Middle America Trench (MAT) and convergence rate shown for Cocos Plate.

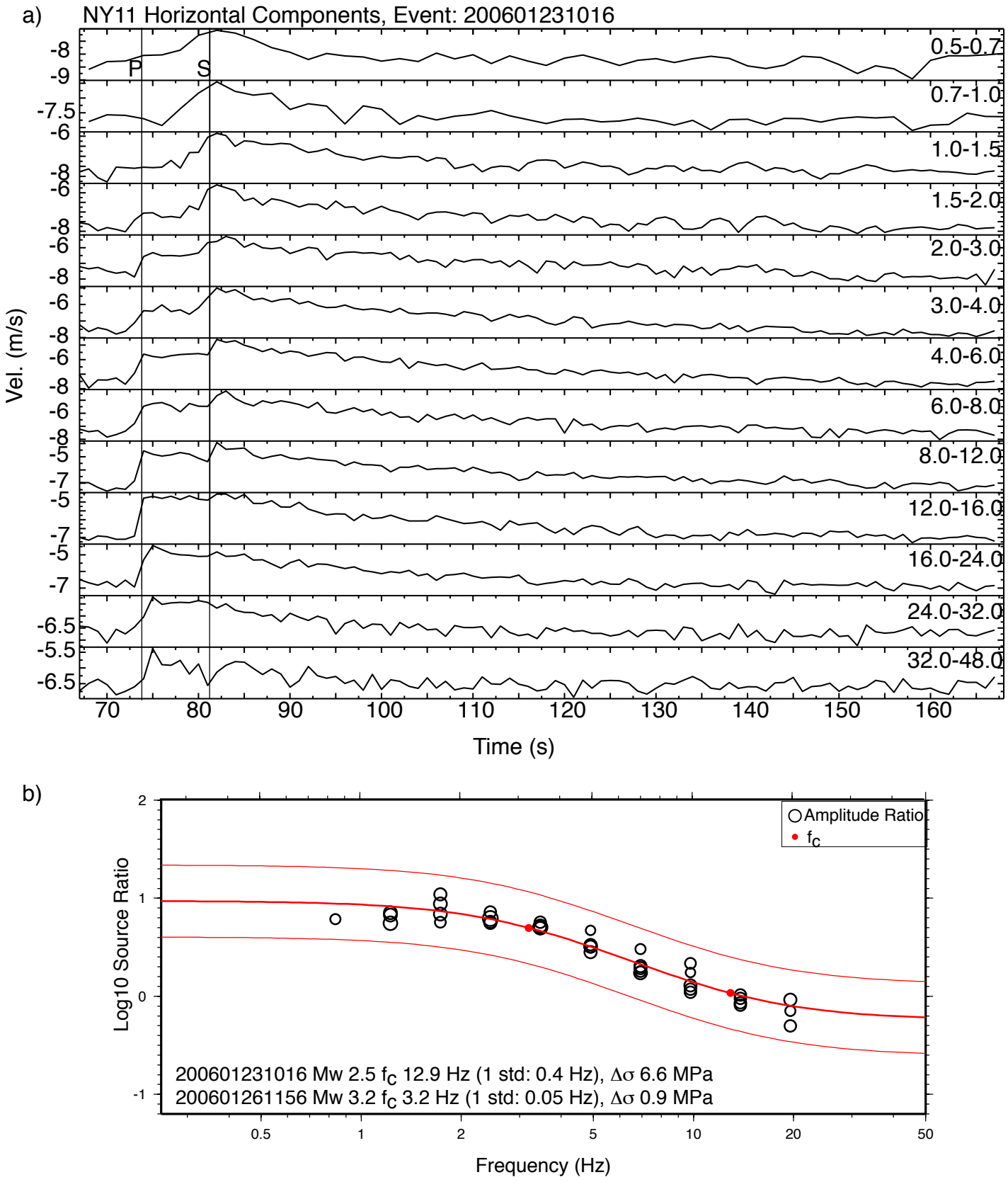

Figure 2: Data processing for January 23, 2006 Mw 2.5 earthquake (cluster c1). a) Envelopes for selected frequency bands 0.5-48 Hz Hz for same event and land station NY11. P and S arrivals are marked with vertical bar. b) Resulting source ratios (open circles) for 2 events, one based on the envelopes shown in a. Solid lines (red) indicate best fit modeled source ratios based on the Brune model, solid circles (red) indicate best fit corner frequency for each event.

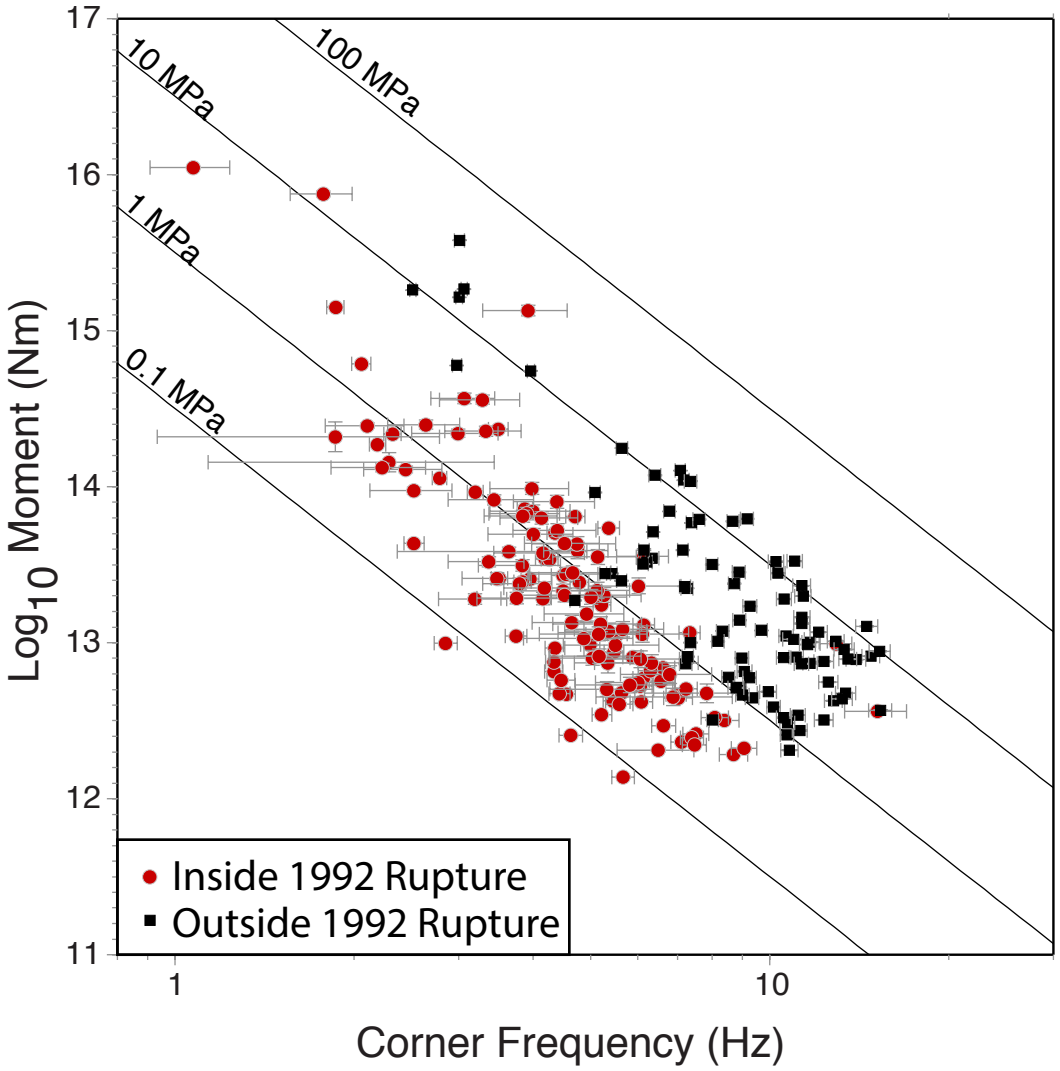

Figure 3: Log moment as function of corner frequency for all events analyzed. Solid lines indicate values of constant stress drop. Events located outside the 1992 rupture area (solid squares) have higher fc and higher $\Delta\sigma$ than events located inside the 1992 rupture area (open circles). Error bars indicate one standard deviation about the mean f_c and M_o resulting from jackknife-based analysis.

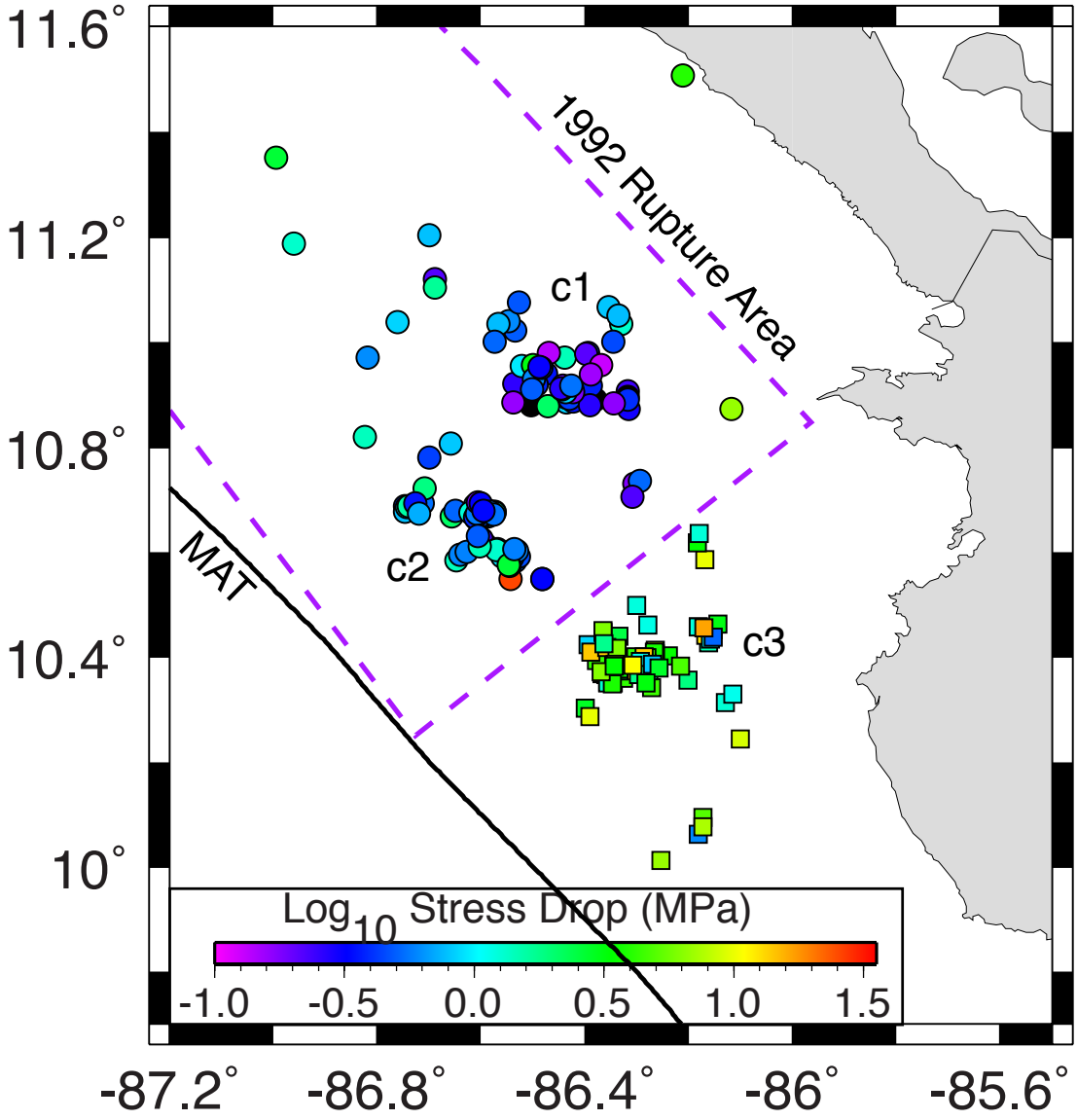

Figure 4: Earthquake stress drop along northern Costa Rica and southern Nicaragua, spanning the southern portion of the 1992 tsunami earthquake rupture zone. Earthquakes outside of the rupture zone (dashed box) have higher $\Delta\sigma$ than those inside the rupture zone. The area of c1 and c2 is within a low rupture velocity, high moment release patch of Ihmlé [1996]; this is also the area of imaged subducted seamount [McIntosh et al., 2007].